



HAL
open science

Inhibitors of UHRF1 base flipping activity showing cytotoxicity against cancer cells

Stefano Ciaco, Viola Mazzoleni, Aqib Javed, Sylvia Eiler, Marc Ruff, Marc Mousli, Mattia Mori, Yves Mély

► **To cite this version:**

Stefano Ciaco, Viola Mazzoleni, Aqib Javed, Sylvia Eiler, Marc Ruff, et al.. Inhibitors of UHRF1 base flipping activity showing cytotoxicity against cancer cells. *Bioorganic Chemistry*, 2023, 137, pp.106616. 10.1016/j.bioorg.2023.106616 . hal-04238876

HAL Id: hal-04238876

<https://cnrs.hal.science/hal-04238876>

Submitted on 12 Oct 2023

HAL is a multi-disciplinary open access archive for the deposit and dissemination of scientific research documents, whether they are published or not. The documents may come from teaching and research institutions in France or abroad, or from public or private research centers.

L'archive ouverte pluridisciplinaire **HAL**, est destinée au dépôt et à la diffusion de documents scientifiques de niveau recherche, publiés ou non, émanant des établissements d'enseignement et de recherche français ou étrangers, des laboratoires publics ou privés.

1 **Inhibitors of UHRF1 base flipping activity showing cytotoxicity against cancer**
2 **cells**

3
4 Stefano Ciaco^{1, 2, #}, Viola Mazzoleni^{1, #}, Aqib Javed¹, Sylvia Eiler³, Marc Ruff³, Marc Mousli^{1, *},
5 Mattia Mori^{2, *}, Yves Mély^{1, *}.

6
7 ¹Laboratoire de Bioimagerie et Pathologies, UMR 7021 CNRS, Université de Strasbourg, Faculté
8 de Pharmacie, Illkirch-France.

9 ²Department of Biotechnology, Chemistry and Pharmacy, Università degli Studi di Siena, Via Aldo
10 Moro 2, 53100, Siena, Italy.

11 ³Institut de Génétique et de Biologie Moléculaire et Cellulaire (IGBMC), INSERM U964 CNRS
12 UMR 7104, Université de Strasbourg, Illkirch, France.

13 [#]These authors contributed equally to this work.

14
15 ^{*}Corresponding authors:

16 Email: Yves Mély: yves.mely@unistra.fr

17 <https://orcid.org/0000-0001-7328-8269>

18 Email: Mattia Mori: mattia.mori@unisi.it

19 <https://orcid.org/0000-0003-2398-1254>

20 Email: Marc Mousli: marc.mousli@unistra.fr

21 <https://orcid.org/0000-0001-9759-6864>

22

23

24

25 **Abstract**

26 Ubiquitin-like containing PHD and RING finger domain 1 (UHRF1) is a nuclear multi-domain
27 protein overexpressed in numerous human cancer types. We previously disclosed the anthraquinone
28 derivative UM63 that inhibits UHRF1-SRA domain base-flipping activity, although having DNA
29 intercalating properties. Herein, based on the UM63 structure, new UHRF1-SRA inhibitors were
30 identified through a multidisciplinary approach combining molecular modelling, biophysical assays,
31 molecular and cell biology experiments. We identified AMSA2 and MPB7, that inhibit UHRF1-SRA
32 mediated base flipping at low micromolar concentrations, but do not intercalate into DNA, which is
33 a key advantage over UM63. These molecules prevent UHRF1/DNMT1 interaction at replication
34 forks and decrease the overall DNA methylation in cells. Moreover, both compounds specifically
35 induce cell death in numerous cancer cell lines, displaying marginal effect on non-cancer cells, as
36 they preferentially affect cells with high level of UHRF1. Overall, these two compounds are
37 promising leads for the development of anti-cancer drugs targeting UHRF1.

38

39 **Keywords:** Epigenetics, DNA methylation; UHRF1 base flipping inhibitors; fluorescence; virtual
40 screening.

41

42

43

44

45

46

47

48

49

50 **Introduction**

51 Cancer is one of the leading causes of death worldwide, accounting for nearly 10 million deaths in
52 2020¹. Despite significant advances, the current anticancer therapies lack of specificity and lead to
53 severe side effects. Furthermore, cancers in advanced stages are characterized by aggressiveness and
54 metastasis, which makes it difficult to control their progression using current anticancer drugs².
55 Importantly, epigenetics is tightly associated to tumorigenesis, being involved in several critical steps
56 ranging from cancer priming, development, progression and metastasis. Dysregulation of epigenetic
57 methylation patterns is a hallmark for cancer³⁻⁷, while disruption of methylation patterns at specific
58 loci, such as tumor suppressor genes (TSGs) promoters, correlates to tumorigenesis⁸⁻¹⁴. As a result,
59 cell cycle (p15^{INK4b}, p14^{ARF}) and DNA repair pathways (hMLH1, MGMT) are altered, inhibiting
60 apoptosis (DAPK) and promoting angiogenesis. In addition, epigenetic alterations can reverse
61 chemotherapy effects¹⁵. Therefore, epigenetic modulators appear as valuable anti-cancer targets¹⁶⁻²².
62 DNA methylation is maintained by a Epigenetic Code Replication Machinery (ECCRM) that
63 faithfully propagates methylation patterns during DNA replication^{18,22}. In this complex, DNA
64 methyltransferase 1 (DNMT1) is guided by Ubiquitin-like, containing PHD and RING fingers
65 domains, 1 (UHRF1) protein. Through its SET and RING-associated (SRA) domain, UHRF1
66 recognizes the CpG motifs of hemi-methylated DNA, which is constituted of the parental methylated
67 DNA strand and the newly synthesized one. Following recognition, the SRA domain flips out the 5-
68 methylcytosine (5mC) of the parent strand from the DNA helix^{23,24}. This base flipping activity
69 triggers DNMT1 recruitment at the replication forks, leading to methylation of the opposite cytosine
70 on the unmethylated strand^{21,22,25}. In addition, through its Tandem Tudor domain (TTD) and plant
71 homeodomain (PHD), UHRF1 interacts with histone 3 (H3) and through its C-terminal RING
72 domain, ubiquitinylates H3K23 and H3K18 residues^{4,23,24,26,27,27-32}. Overall, UHRF1 plays a pivotal
73 role in G₁/S transition^{33,34} and the epigenetic silencing of tumor suppressor genes (TSGs) such as
74 p16^{INK4A}, p14^{ARF}, BRCA1, RB1, KISS1, RASSF1, CDKN2A and RAR α ^{10,12,16-19,35-39}. As UHRF1 is

75 a well-known oncogene overexpressed in numerous human cancer types^{10,18}, pharmacological
76 inhibition of UHRF1 activity or expression represents a promising perspective in anticancer therapy
77 to reactivate silenced TSGs, and induce apoptosis^{10,40}.

78 Currently, several therapeutic strategies aim to inhibit DNA methylation in cancer cells⁴¹.
79 Demethylating compounds include nucleoside (5-azacytidine and decitabine)^{42,43} and non-nucleoside
80 analogs (Hydralazine and Procainamide)⁴⁴ but show strong drawbacks, such as chemical instability,
81 cytotoxicity on non-cancer cells and poor selectivity for DNMT1⁴⁵⁻⁴⁷. Due to the high expression of
82 UHRF1 in cancer cells and its key activity on TSGs, UHRF1 represents a promising anticancer target
83 for the development of DNA methylation modulators that might bear better features than current
84 demethylating drugs^{48,49}. So far, several natural and synthetic inhibitors of UHRF1 have been
85 reported, including uracil derivatives⁵⁰, 4-benzylpiperidine-1-carboximidamide⁵¹, mitoxantrone,
86 anthracycline inhibitors of topoisomerase II⁵²⁻⁵⁴ and UM63⁵⁵. This last compound shares some
87 chemical features with mitoxantrone, and inhibits UHRF1 in the low micromolar range by binding to
88 5mC binding pocket of SRA⁵⁵. Moreover, UM63 prevents DNMT1/UHRF1 interaction and decreases
89 DNA methylation in HeLa cells proving the druggability of the SRA binding pocket. However, the
90 DNA intercalating properties of UM63 represent a weakness that should be absent in next generations
91 of UHRF1 inhibitors. Recently, UF146, another UHRF1 inhibitor targeting SRA domain was
92 identified. This compound was shown to efficiently eradicate leukemia initiating cells in a myeloid
93 leukemia patient-derived xenograft model, confirming the high potential of UHRF1 inhibitors in
94 anticancer therapy⁵⁶. UF146 is structurally related to UM63 and mitoxantrone, but unfortunately it
95 qualifies as a pan-assay interference compounds (PAINS)^{57,58} due to its quinone moiety. Noteworthy,
96 PAINS are molecules bearing undesired functional groups that might react unpredictably with
97 numerous biological targets rather than with the desired target, giving rise to false positive results⁵⁸.

98 In this context, the aim of this work was to identify and characterize improved potent UHRF1
99 inhibitors based on UM63 pharmacophoric features through a combination of molecular modeling,
100 biophysical assays and biological studies. Two effective UHRF1 inhibitors, i.e., the

101 hydroxyanthracene derivative AMSA2 (namely, anthrarobin) and the imidazoquinoline derivative
102 MPB7, were identified. Both compounds prevent SRA-induced base flipping, decrease the overall
103 DNA methylation in cancer cells, do not qualify as PAINS, and are not DNA intercalators, thus
104 becoming promising compounds for anticancer applications.

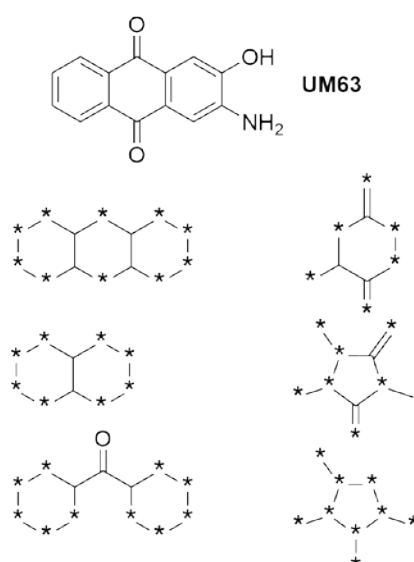
105

106 Results

107 Hits selection by virtual screening

108 To identify different chemotypes that might bind into the 5mC binding pocket of the SRA domain,
109 the Aldrich Market Select and MolPort databases were screened *in silico*. Based on the chemical
110 structure of UM63 and its substructures, i.e., an effective UHRF1 inhibitor that binds the 5mC pocket
111 of SRA previously disclosed by our group⁵⁵, a SMARTS-based pre-filtration of the databases was
112 carried out (**Fig. 1**). Specifically, SMARTS patterns were designed to preserve the major
113 pharmacophores or functional groups that were thought to be relevant for UM63 binding to SRA
114 domain. These include large structures such as the tricyclic anthracene-like core that mimics UM63,
115 as well as simplified structures to enhance chemical diversity in the final screening library.

116



117

118 **Figure 1:** Chemical structure of UM63 and its substructures that were used in the generation of SMARTS patterns for
119 chemical databases pre-filtration. * represents any connected atom including H.

120

121 By database pre-filtration through SMARTS patterns, ~1.3 and ~3.7 million molecules were selected
122 from Aldrich Market Select and MolPort (around 15% and 48% of the initial databases, respectively)
123 which were submitted to molecular docking with FRED program from OpenEye (FRED 3.0.1:
124 OpenEye Scientific Software, Santa Fe, NM. <http://www.eyesopen.com>)⁵⁹. The X-ray
125 crystallographic structure of the human SRA domain of UHRF1 bound to hemi methylated (HM)
126 DNA was used as a rigid receptor (PDB_ID: 3CLZ)⁵⁹. Based on FRED Chemgauss4 score, top
127 ranking 1000 compounds were selected for further investigations. Among them, a few derivatives
128 share the main scaffold with UM63, while others have different chemotypes, including naphthalene,
129 benzoic acid, carbamide, guanidine, and various heterocyclic derivatives. To maximize chemical
130 diversity in the final selection of virtual hits, these 1'000 top ranking virtual hits were further clustered
131 based on a combination of fingerprints and substructure search through a well-established
132 cheminformatics approach⁶⁰⁻⁶². Finally, combining visual inspection of docking poses with chemical
133 diversity analysis led to the selection of 27 virtual hits from Aldrich Market Select (**Fig. S1**) and 37
134 virtual hits from MolPort (**Fig. S2**), which were submitted to experimental validation.

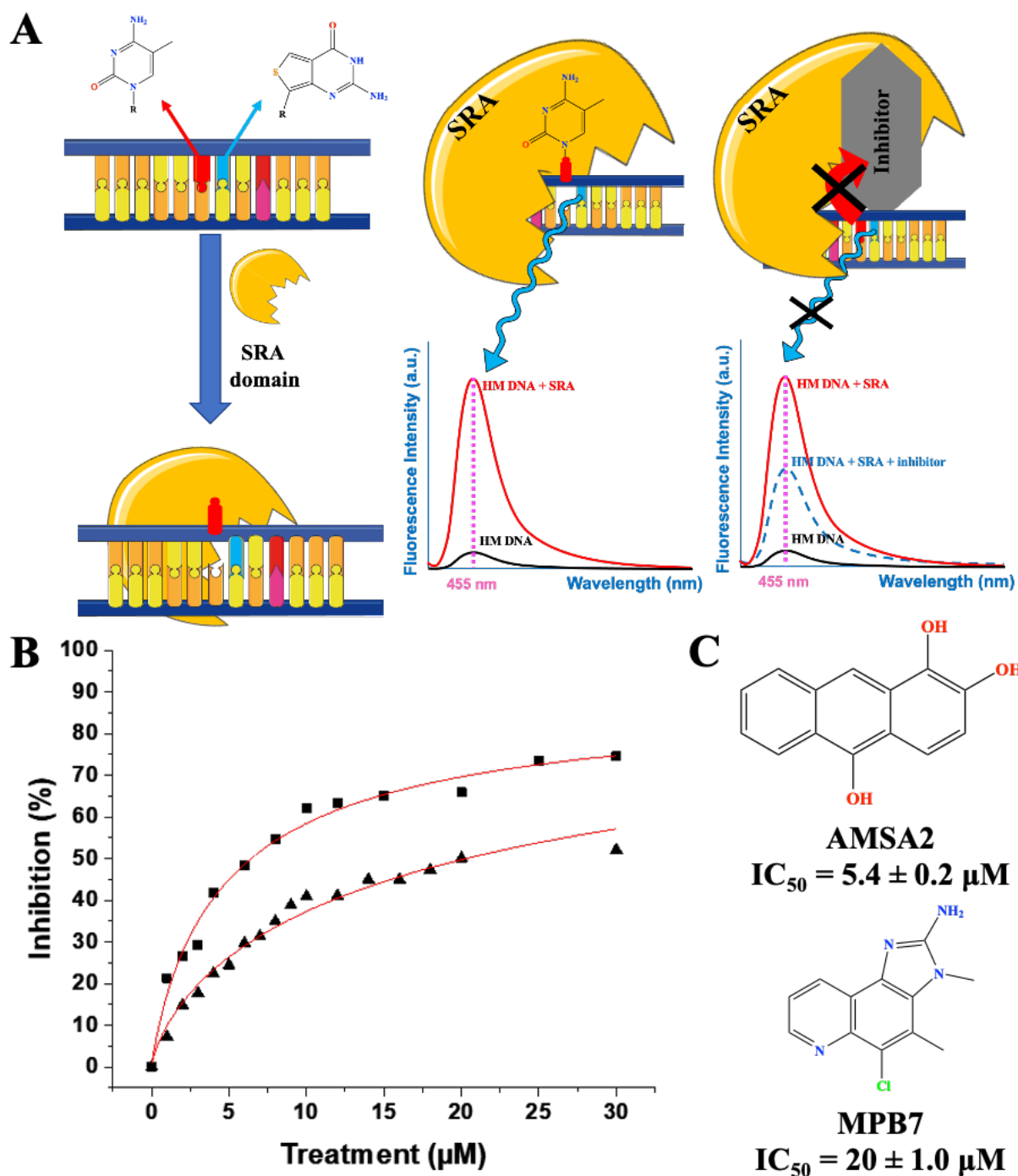
135

136 ***In vitro* screening and characterization of virtual hits**

137 The 64 compounds selected by virtual screening were then tested *in vitro* using a highly sensitive
138 fluorescence-based assay that monitors the 5mC base flipping activity. This assay takes advantage of
139 the photophysical features of thienoguanosine (thG), an isomorphous guanosine surrogate⁶³⁻⁶⁵,
140 incorporated into the 12-bp duplex whose structure in complex with SRA has been solved by X-ray
141 crystallography²⁴. In this HM duplex, thG was used to replace the G residue at position 7 in the single
142 CpG site (**Fig. 2A**). thG perfectly replaces G in this duplex and sensitively responds to the SRA-
143 induced base flipping of the flanking 5mC with a strong fluorescence increase^{66,67}. Therefore, a small
144 molecule able to bind into the 5mC binding pocket of SRA can be identified through a decrease of
145 the thG fluorescence intensity (**Fig. 2B**).

146 By monitoring the base flipping interference of the 64 virtual hits at 10 μM , ten compounds showed
147 an inhibitory effect $> 30\%$ and were selected for further analyses (**Table S1**). Next, the dose-response
148 curves of the 10 selected compounds were recorded on the SRA-induced base flipping assay (**Table**
149 **S2**). In parallel, as DNA intercalating properties of UM63 were a major drawback, we also tested
150 their DNA intercalating properties by competition with ethidium bromide (EtBr) for the HM DNA
151 duplex (UM63 intercalation data from Zaayter et al, 2019 are reported in **Fig. S3**, blue triangles).
152 From these two assays, we selected the most efficient compounds with an IC_{50} value $\leq 20 \mu\text{M}$ on the
153 base flipping assay and $< 20\%$ ejection of EtBr at 30 μM concentration (**Table S2**). This combination
154 of assays allowed to prioritize three compounds, i.e. AMSA2, AMSE2 and MPB7. Among them,
155 AMSA2 and AMSE2 are structurally related to UM63, with which they also share comparable IC_{50}
156 values ($5.4 \pm 0.2 \mu\text{M}$, $4.5 \pm 0.2 \mu\text{M}$ and $4.4 \pm 0.5 \mu\text{M}$ for AMSA2, AMSE2 and UM63, respectively).
157 UM63 IC_{50} data Zaayter et al, 2019 are reported in **Fig. S3**, green squares. Since AMSE2 is
158 structurally related to benzo[*a*]pyrene, a carcinogenic agent that can cause skin, lung, and bladder
159 cancer in humans and in animals⁶⁸, this compound was discarded. MPB7 exhibits a slightly higher
160 IC_{50} ($20 \pm 1.0 \mu\text{M}$) compared to AMSA2, and it is a member of imidazoquinoline family, which is a
161 class of immunomodulatory drugs with anticancer features⁶⁹⁻⁷². Accordingly, we focused following
162 studies on AMSA2 and MPB7 (**Fig. 2C**), which both show remarkable inhibition of UHRF1 base
163 flipping activity and marginal DNA intercalating ability, thus overcoming the major limitation of
164 UM63.

165



166
 167
 168
 169
 170
 171

Figure 2: *In vitro* screening of virtual hits preventing SRA-induced base flipping. (A) Principle of the base flipping assay. (B) Dose-response curves of AMSA2 (black squares) and MPB7 (black triangles). The red lines correspond to the fit of the data points with equation 2 from Materials and Methods. (C) AMSA2 and MPB7 structures and their IC_{50} values determined from the fits in panel B.

172 We then evaluated the ability of AMSA2 and MPB7 to dissociate the SRA/HM DNA complex, by
 173 monitoring the fluorescence anisotropy of the fluorescein-labelled HM duplex. In its free form, the
 174 labelled duplex exhibited a very low anisotropy value (~0.016) while, in complex with SRA, the
 175 anisotropy value increased to 0.17. Addition of increasing concentrations of AMSA2 and MPB7 up

176 to 200 μ M only slightly decreases the anisotropy value (**Fig. S4**), indicating that AMSA2 and MPB7
177 inhibit SRA-induced base flipping, without dissociating the SRA/HM DNA complex.

178

179 **Binding mode of AMSA2 and MPB7 in the SRA binding pocket**

180 To further assess the interaction of AMSA2 and MPB7 with the 5mC binding pocket of SRA,
181 molecular docking simulations were carried out using more extensive sampling parameters compared
182 to virtual screening.

183 Both molecules establish H-bonds with key residues of UHRF1 that are known to interact with the
184 flipped 5mC as well as with the backbone of HM DNA²⁴, such as Val446, Ala463, Gly465, Asp469,
185 and Thr479 (**Fig. 3**). The aromatic ring of both compounds is π -stacked to the side chain of Tyr478
186 in a parallel-displaced orientation. Similar to the binding mode of 5mC in the X-ray crystallography
187 structure, the side chain of Tyr466 establishes hydrophobic/aromatic interactions with the compounds
188 on the opposite side compared to Tyr478. The catechol moiety of AMSA2 establishes an extensive
189 network of H-bond interactions with the backbone of Ala463 and Thr479, as well as with the side
190 chain of Asp469 (**Fig. 3A**), while the isolated hydroxyl group is H-bonded to the backbone of Val446.
191 The aminoimidazole moiety of MPB7 is largely engaged in H-bonds with the backbone of Ala463
192 and Gly465, while it interacts with the side chain of Asp469 (**Fig. 3B**). Overall, these binding modes
193 strongly overlap with the binding mode of the natural substrate 5mC (**Fig. 3C and Fig. S5**), which
194 might provide a structural explanation to the inhibitory effects of AMSA2 and MPB7 as observed in
195 experimental studies.

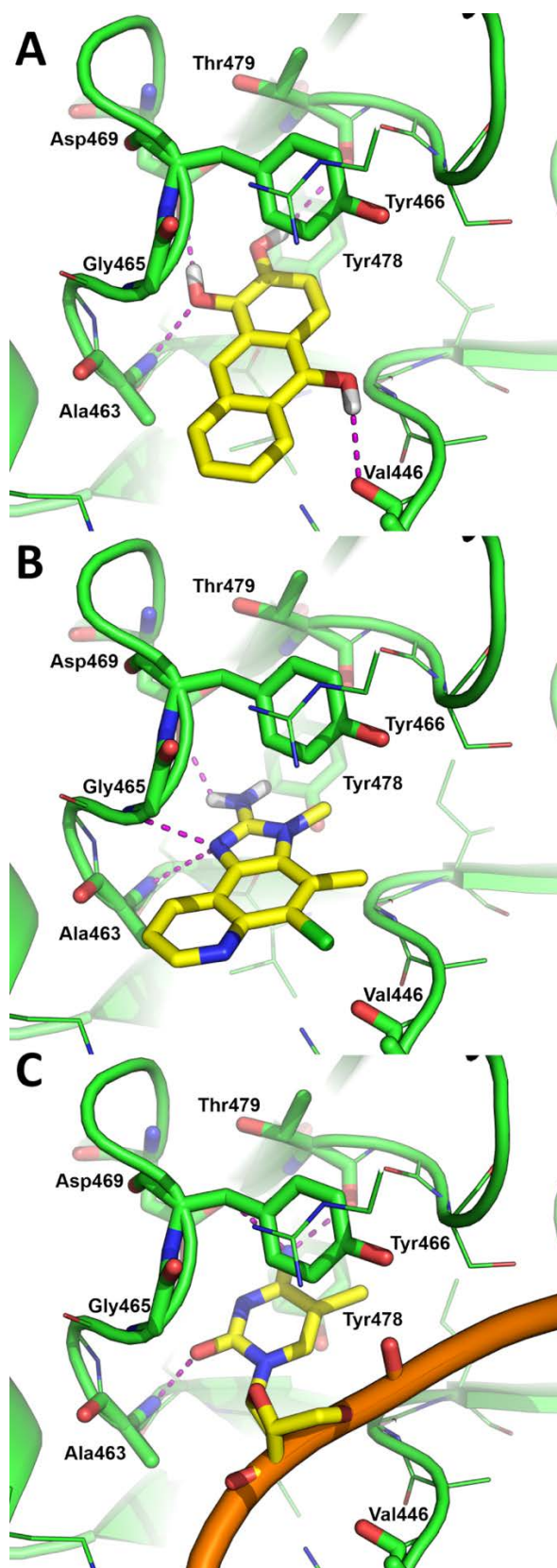


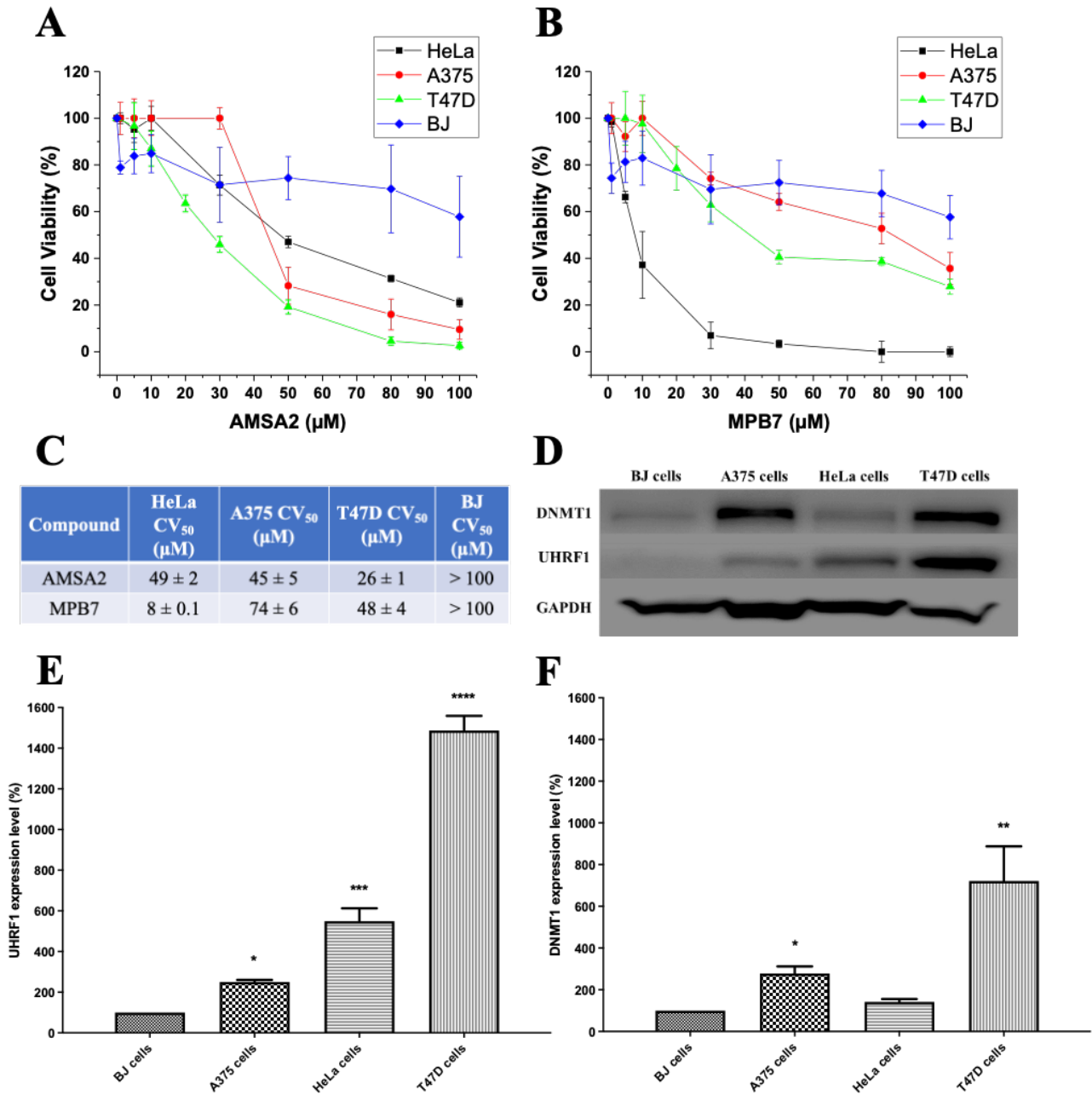
Figure 3: Docking-based binding mode of AMSA2 (A) and MPB7 (B) and X-ray crystallography pose of 5mC (C) within the 5mC binding site of SRA. AMSA2, MPB7, and 5mC are shown as yellow sticks while the crystallographic structure of SRA (PDB_ID: 3CLZ) is shown as green cartoon. Residues within 5 Å from the ligands are shown as lines, while those contacted by the inhibitors and discussed in the main text are labelled and shown in sticks. H-bond interactions are highlighted by magenta dashed lines.

196
197
198
199
200
201
202

203 **AMSA2 and MBP7 decrease cancer cell viability in correlation with UHRF1 expression level**

204 The effect of AMSA2 and MPB7 on the viability of cervical cancer cells (HeLa), melanoma cancer
205 cells (A375) and breast ductal carcinoma cells (T47D) expressing different UHRF1 levels¹⁰ was
206 tested for 48 h by using the MTT assay. Selected compounds were also tested on healthy foreskin
207 fibroblasts (BJ). Notably, both compounds show a dose-dependent effect on cancer cells with only
208 marginal effects on BJ cells (**Fig. 4A** and **B**). Previous cell viability data from UM63⁵⁵ were added
209 in **Fig. S3**, red circles. Evaluation of the concentrations leading to a 50% decrease in cell viability
210 (CV_{50}) (**Fig. 4A** and **B**) revealed that MPB7 ($CV_{50} \sim 8 \mu\text{M}$) was more active than AMSA2 ($CV_{50} \sim 49$
211 μM) or UM63 ($CV_{50} \sim 30 \mu\text{M}$)⁵⁵ on HeLa cells. In contrast, MPB7 was two-fold less active than
212 AMSA2 on A375 and T47D cells. Finally, both compounds show low impact on the viability of BJ
213 cells ($CV_{50} > 100 \mu\text{M}$).

214



215
216
217
218
219
220
221
222
223
224
225
226

Figure 4: Effect of AMSA2 and MPB7 on cell viability (A-C), and correlation with UHRF1 and DNMT1 expression levels (D-F). Cell viability on treatment with AMSA2 (A) and MPB7 (B) was investigated using a MTT assay. HeLa, A375, T47D and BJ data points are shown as black squares, red circles, green triangles and blue diamonds, respectively. Each concentration has been tested in hexaplicate with at least 3 different biological replicates. In the Table of panel C, the concentrations leading to a 50% decrease in cell viability (CV₅₀) were deduced from the curves in panels A and B. (D) Western blots and (E) UHRF1 expression level and (F) DNMT1 expression level. Western blot images were processed with ImageJ software and the intensity of each band was normalized to the corresponding GAPDH band. The results between groups were statistically compared by one-way ANOVA with post-hoc Bonferroni test using GraphPad-Prism (version 5.04) software. Statistical significance is represented as *ns* > 0.05, **p* < 0.05, ***p* < 0.01, and *****p* < 0.0001 versus control.

227 As both compounds were selected based on their ability to inhibit UHRF1, we next investigated
228 whether their differential effect on healthy and cancer cells depends on UHRF1 expression levels
229 (**Fig. 4D**). In line with the preferential effect of the compounds on the viability of cancer cells, UHRF1
230 expression was significantly higher in cancer cell lines as compared to BJ cells (**Fig. 4E**). Concerning
231 DNMT1, its expression level was low in both BJ and HeLa cells, which poorly correlates with the
232 observed effects on cell viability (**Fig. 4F**). Taken together, our data are in line with the hypothesis
233 that both compounds may impair cell viability by targeting UHRF1. Since HeLa cells were found to
234 be particularly sensitive to MPB7, they were selected for further investigations.

235

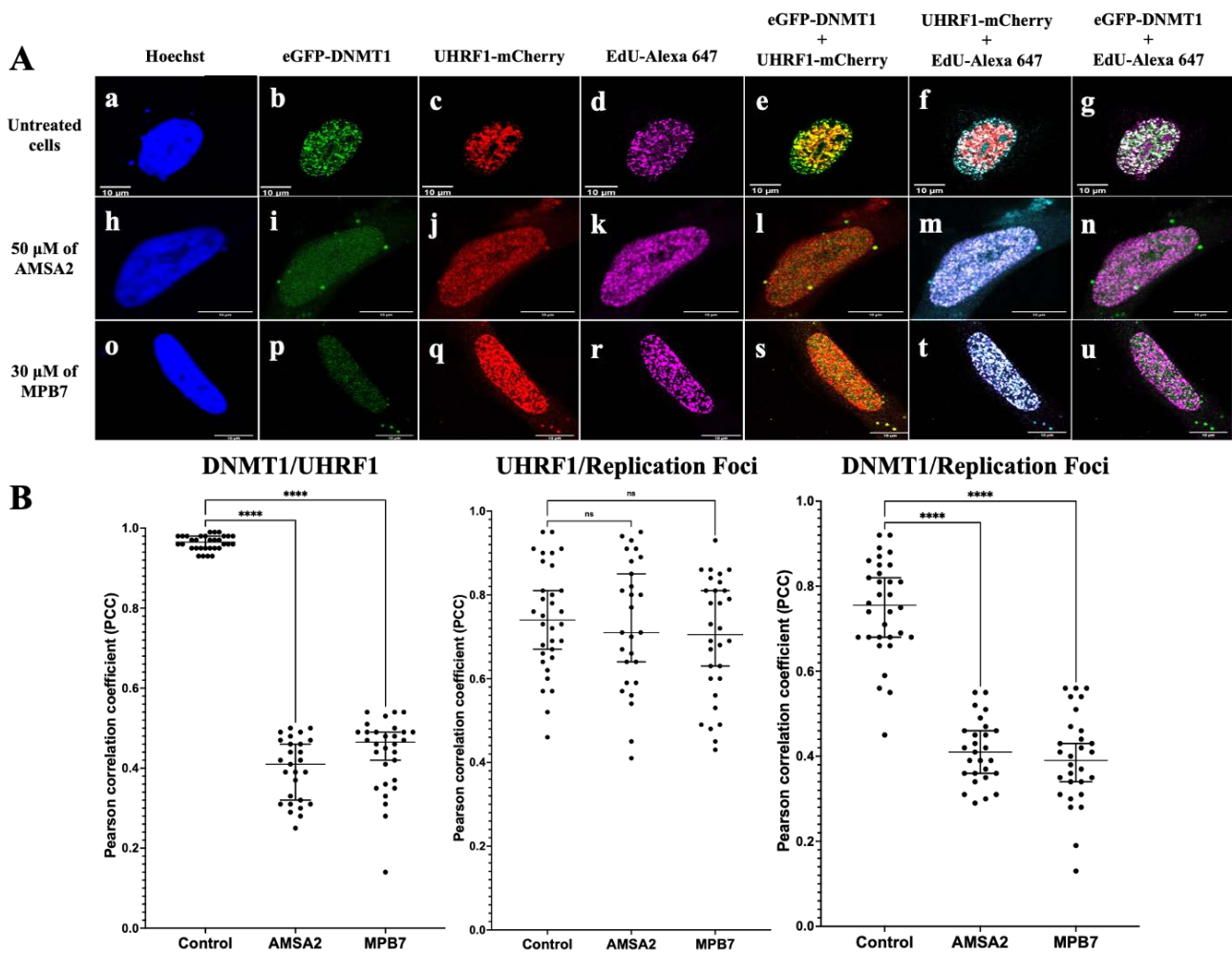
236 **AMSA2 and MBP7 prevent DNMT1 recruitment at the replication foci**

237 To confirm that AMSA2 and MBP7 target UHRF1 in cancer cells, we investigated by confocal
238 microscopy their ability to impact UHRF1 functions in cells. UHRF1 has been previously shown to
239 recruit DNMT1 onto the replication foci^{21,22,55,73,74}, a function that is inhibited by UM63⁵⁵. To
240 evaluate if AMSA2 and MPB7 exhibit similar properties, we transiently transfected HeLa cells with
241 eGFP-DNMT1 and UHRF1-mCherry and then analyzed the co-localization of the two proteins at the
242 replication foci in the presence of 30 μ M of MPB7 and 50 μ M of AMSA2 after 24 h of treatment.
243 These two concentrations were chosen based on the dose-response curves of the two compounds on
244 HeLa cells (**Fig. 4A** and **B**). HeLa cells were additionally labeled with both EdU-Alexa647 and
245 Hoechst dye, to highlight the replication foci and nuclei, respectively (**Fig. 5**).

246 In non-treated HeLa cells, both UHRF1 and DNMT1 were well co-localized at the replication foci
247 (yellow dots, **Fig. 5** panel **e**), in full line with previous observations^{21,22,25,55,74}. AMSA2 and MPB7
248 had no effect on the localization of UHRF1 at replication foci (**Fig. 5** panels **m** and **t**), as confirmed
249 by the unchanged Pearson Correlation Coefficient (PCC) between UHRF1-mCherry and Edu (**Fig.**
250 **5B**). The marginal impact of the compounds on the localization of UHRF1 at the replication foci is
251 consistent with our anisotropy data (**Fig. S5**), suggesting that AMSA2 and MPB7 do not dissociate
252 SRA/HM DNA complexes. In contrast, AMSA2 and MPB7 induced a significantly decreased co-

253 localization between DNMT1 and UHRF1 signals (**Fig. 5** panels **l** and **s**) associated with a decrease
254 of DNMT1 localization at the replication foci (**Fig. 5** panels **n** and **u**). This was confirmed by the
255 significant PCC decrease for the overlap of the two labelled proteins (0.99 ± 0.01 in non-treated cells
256 vs 0.4 ± 0.01 in treated cells, **Fig. 5B**) and the overlap of eGFP-DNMT1 and EdU signals ($0.79 \pm$
257 0.05 in non-treated cells vs 0.4 ± 0.01 in cells treated with the hits, **Fig. 5B**).

258 In conclusion, our data show that both AMSA2 and MPB7 inhibit DNMT1 recruitment onto
259 replication foci, likely as a result of UHRF1 base flipping inhibition.



260
 261 **Figure 5:** AMSA2 and MPB7 effect on DNMT1/UHRF1 co-localization onto replication foci. (A) Confocal images
 262 showing eGFP-DNMT1 and UHRF1-mCherry distribution in HeLa cells labeled with EdU-Alexa 647 and Hoechst
 263 dye. Panels **a** to **g** correspond to untreated cells (control), **h** to **n** correspond to cells treated with AMSA2 at 50 μ M and
 264 to **o** to **p** correspond to cells treated with MPB7 at 30 μ M. **a**, **h** and **o** panels show Hoechst dye (nucleus). **b**, **i** and **p** panels
 265 show eGFP-DNMT1. **c**, **j** and **q** panels show UHRF1-mCherry. **d**, **k** and **r** panels show EdU-Alexa 647 (replication foci
 266 in S Phase). **e**, **l** and **s** panels show co-localization of eGFP-DNMT1 with UHRF1-mCherry. **f**, **m** and **t** panels show the
 267 localization of eGFP-DNMT1 onto replication foci (Edu-Alexa 647). **g**, **n** and **u** panels show the localization of UHRF1-
 268 mCherry onto replication foci (Edu-Alexa 647). White bar indicates size of 10 μ m. (B) Dot plot representation of the
 269 Pearson correlation coefficient (PCC) values for the co-localization of DNMT1/UHRF1, UHRF1/Foci and DNMT1/Foci
 270 in the confocal images. Each dot corresponds to one cell. The total number of analyzed cells was 30 for control, AMSA2
 271 at 50 μ M and MPB7 at 30 μ M from at least three different biological replicates. Results between groups were statistically
 272 compared by one-way ANOVA with post-hoc Bonferroni test using GraphPad-Prism (version 5.04) software. Statistical
 273 significance is represented as *ns* > 0.05, **p* < 0.05, ***p* < 0.01, and ****p* < 0.001, *****p* < 0.0001 versus control.
 274

275 **Inhibition of SRA base flipping is associated with a drop in global DNA methylation level**

276 We next investigated whether AMSA2 and MPB7 affects the global DNA methylation of HeLa cells
277 after 48 h of treatment by using an immunofluorescence assay with a specific monoclonal antibody
278 against 5mC (**Fig. 6A**). As a positive control, we treated HeLa cells with 100 μ M of 5-azacytidine,
279 an FDA-approved DNMT1 inhibitor, which leads to 83% decrease of 5mC fluorescence compared to
280 untreated cells.

281 AMSA2 was observed to reduce global DNA methylation by only 10% at 10 μ M concentration but
282 by 75% at 50 μ M (**Fig. 6B**). A stronger effect was observed with MPB7, which decreased the global
283 methylation level by 87% and 93% at 10 and 30 μ M, respectively. Therefore, MPB7 at 10 μ M and
284 AMSA2 at 50 μ M efficiently decreased 5mC fluorescence, similarly to 100 μ M of azacytidine,
285 suggesting that both inhibitors of UHRF1 base flipping effectively decrease the methylation level in
286 cancer cells.

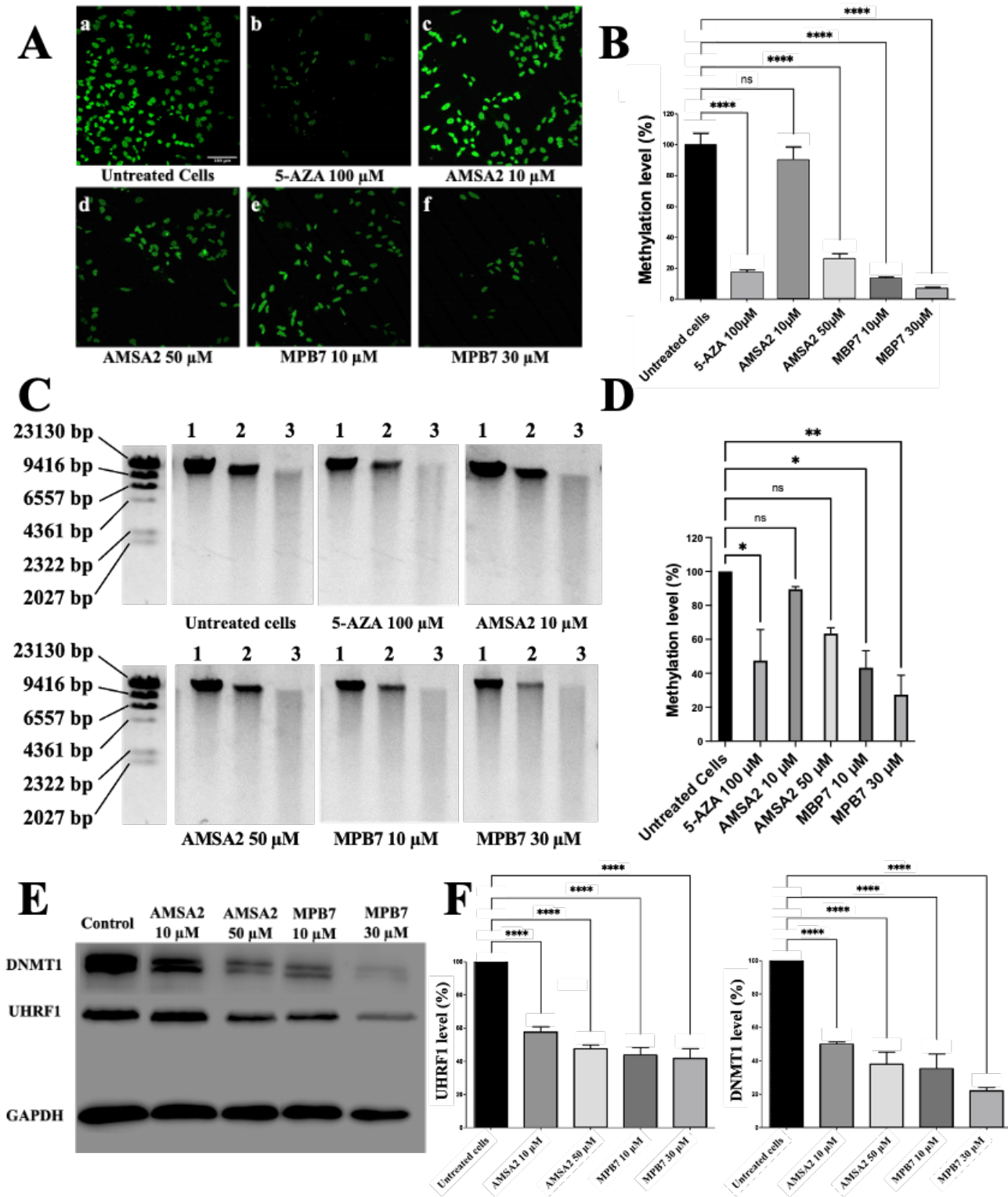
287 We also confirmed the effect after 48 h of treatment with AMSA2 and MPB7 on global DNA
288 methylation with digestion by methyl sensitive and insensitive restriction endonucleases, *HpaII* and
289 *MspI*, respectively (**Fig. 6C**). HeLa cells treated with 100 μ M of 5-azacytidine was used as positive
290 control. As a result, AMSA2 reduced the global DNA methylation by 11% at 10 μ M and 37% at 50
291 μ M, while a stronger effect was observed with MPB7, which decreased the global methylation level
292 by 58% and 74% at 10 and 30 μ M, respectively (**Fig. 6D**). 100 μ M of 5-azacytidine led to 47%
293 decrease.

294 At this stage, the molecular mechanisms that link the initial inhibition of UHRF1 base flipping
295 activity by AMSA2 and MPB7 and the decrease of DNA methylation observed at 48 h are unknown.

296 Among the possible scenarios, a decrease in DNMT1 protein level could be an obviously possible
297 step in these mechanisms. To check this hypothesis, we monitored UHRF1 and DNMT1 protein
298 levels after AMSA2 and MPB7 treatments for 48 h (**Fig. 6E**). A very significant decrease in both
299 UHRF1 and DNMT1 protein levels was observed with both compounds (**Fig. 6F**), suggesting that

300 part of the observed decrease in the global DNA methylation level might be due to a decrease in
 301 DNMT1 protein level in the treated cells.

302



303 **Figure 6:** AMSA2 and MPB7 effect on global methylation level in HeLa cells, as evaluated by using labelled monoclonal
 304 antibody against 5mC (A, B), methylation sensitive enzymes (C, D) and effect on UHRF1 and DNMT1 protein levels (E,
 305 F). (A) Confocal immunofluorescence images showing untreated cells (panel a), cells treated with 100 µM of 5-
 306 azacytidine (panel b), cells treated with 10 µM (panel c) and 50 µM (panel d) of AMSA2 and cells treated with 10 µM
 307

308 (panel e) and 30 μ M (panel f) of MPB7 for 48 h. (B) Quantification of the methylation level from the confocal data. 30
309 pictures for each treatment were analyzed along with controls from at least 3 different biological replicates. (C) Gel
310 images showing digested DNA from untreated cells, cells treated with 100 μ M of 5-azacytidine, 10 μ M and 50 μ M of
311 AMSA2 and 10 μ M and 30 μ M of MPB7 for 48 h; **column 1**, undigested DNA; **column 2**, DNA digested with *HpaII*
312 (methylation sensitive restriction endonuclease); **column 3**, DNA digested with *MspI* (methylation insensitive restriction
313 endonuclease). (D) Quantification of the DNA methylation levels from the enzymatic assay performed on two biological
314 replicates. Gel images were processed with ImageJ software and the intensity of each band was compared to the
315 corresponding band in untreated cells. (E) Western blots showing UHRF1 and DNMT1 protein levels in untreated HeLa
316 cells (control), and in HeLa cells treated with 10 μ M and 50 μ M of AMSA2 or with 10 μ M and 30 μ M of MPB7 for 48
317 h. (F) Quantification of UHRF1 and DNMT1 protein levels from western blot data performed on at least 3 different
318 biological replicates. Gel images were processed with ImageJ software. The intensity of each protein band was normalized
319 to the intensity of the corresponding GAPDH band and then compared to the intensity of the corresponding protein band
320 in untreated cells. Data between groups were statistically compared by one-way ANOVA with post-hoc Bonferroni test
321 using GraphPad-Prism (version 5.04) software. Statistical significance is represented as *ns* > 0.05, * *p* < 0.05, ** *p* < 0.01,
322 and *** *p* < 0.001, **** *p* < 0.0001 versus control.
323

324 Discussion

325 Epigenetic marks govern cell identity by controlling the expression of specific genes. UHRF1 is a
326 key player in the maintenance of epigenetic patterns by orchestrating DNA methylation and
327 recognition of histone modifications. Importantly, while UHRF1 expression is globally low in non-
328 cancer cells, peaking only in G₁ and G₂/M phase³³, it is found overexpressed throughout the cell cycle
329 in several types of human cancers, promoting cell proliferation and dedifferentiation¹⁰. The
330 importance of UHRF1, in particular its SRA domain, is highlighted from mutagenesis experiments
331 in which embryonic stem cells (ESCs) with UHRF1-knockout show DNMT1 dissociation from
332 chromatin^{21,22,75} and UHRF1-deficient embryos show global demethylation and lethality after
333 granulation²¹. Therefore, UHRF1 appears as a valuable target for the development of anticancer
334 agents that impact cancer cells with a high specificity over non-cancer cells.

335 Since DNMT1 recruitment onto replication foci is triggered by 5mC base flipping at HM CpG sites
336 induced by the SRA domain of UHRF1^{21,22,24,76}, our strategy was to target the 5mC binding pocket
337 of SRA using a multidisciplinary approach combining molecular modelling, biophysical assays and
338 molecular and cellular biology. Two molecules, i.e., AMSA2 (1,2,10-trihydroxyanthracene,
339 anthrarobin) and MPB7 (2-amino-5-chloro-3,4-dimethyl-3H-imidazo[4,5-*f*]quinoline) were
340 highlighted as efficient inhibitors of SRA-mediated base flipping. AMSA2 shares the anthracene core
341 with the parent UM63, confirming the importance of anthracene/anthraquinone scaffold to target the

342 SRA base flipping activity^{40,54,55,77}. MPB7 is a member of imidazoquinoline family, a class of
343 immunostimulant drugs with pro-apoptotic properties⁶⁹⁻⁷². These two molecules have activities
344 comparable to UM63 in inhibiting SRA base flipping, but do not show any significant DNA
345 intercalating properties, which is a key advantage over UM63. Indeed, though several anticancer
346 compounds are DNA intercalators, their mechanism of action *in cellulo* is unpredictable, as they can
347 trigger genome damages and mutagenesis through binding to unspecific DNA sequences, which could
348 lead to several adverse effects including cancerogenesis⁷⁸.

349 Molecular modelling revealed that AMSA2 and MBP7 bind similarly to 5mC within the SRA binding
350 pocket, which explains their ability to prevent the SRA-mediated base flipping of 5mC. Moreover,
351 AMSA2 and MPB7 are projected towards the solvent-accessible area near the entrance of the SRA
352 binding pocket. As a consequence, the distal phenyl ring of AMSA2 and the pyridine ring of MPB7
353 were near the entrance of the 5mC binding site and represented thus a potential site for further hit-to-
354 lead optimization (**Fig. S5**).

355 Interestingly, AMSA2 and MPB7 only marginally dissociated the SRA/HM DNA complex,
356 suggesting that they might form a ternary complex while inhibiting base flipping activity. By
357 preventing 5mC flipping in the bound CpG motif, these compounds might perturb UHRF1
358 conformational switch into its active form^{28,55,66,79} thus inhibiting the E3-ligase activity of the RING
359 domain^{29,80,81} and the recruitment of DNMT1, ultimately leading to a DNA methylation decrease.

360 This scenario has been validated in HeLa cell model, evidencing that both compounds inhibit DNMT1
361 recruitment onto replication foci, which ultimately led through a still unknown pathway to a
362 significant decrease in DNA global methylation. UHRF1 inhibition was also confirmed by the effect
363 of both compounds on cell viability, which depended on UHRF1 expression level. Indeed, both
364 compounds efficiently decreased the cell viability of the three tested cancer cell lines overexpressing
365 UHRF1 (HeLa, A375 and T47D), but did not significantly impact non-cancer BJ cells, which display
366 low expression of UHRF1.

367 The cascade of events between the initial inhibition of UHRF1 base flipping by AMSA2 and MPB7
368 and the decrease in cell viability as well as DNA methylation observed after 48 h is still unknown.
369 Nevertheless, our data strongly suggest that part of the decrease in global DNA methylation could be
370 related to the decrease in DNMT1 protein level, probably as a result of its degradation by the
371 proteasome. Studies are in progress to further identify the molecular pathways underlying the activity
372 of the two compounds on DNA methylation and cell viability in relation to their inhibitory activity
373 on UHRF1.

374 To date, FDA approved a few drugs, such as nucleoside analogues 5-azacitidine and decitabine⁴¹⁻⁴⁴,
375 aiming to control DNA hypermethylation by inhibiting DNMT1 activity. These drugs are
376 incorporated in both DNA and RNA during the S phase substituting the Cs. Upon incorporation, these
377 two drugs form a covalent bond in the presence of DNMT1, driving it to proteasome degradation^{82,83}.
378 Due to their mechanism of action and given the very high structural similarity with natural
379 nucleosides, these drugs exhibit a poor therapeutic index and selectivity, as they can be incorporated
380 in both cancer and non-cancer cells.

381 Furthermore, natural products such as flavonoids have been reported to downregulate UHRF1 and
382 consequently to reduce global DNA methylation in HeLa cells^{38,84}. These molecules were thus
383 identified as potential UHRF1 inhibitors, but their mechanism of action is still unclear and none of
384 them reached yet the clinical phase⁵⁰⁻⁵⁵. Recently, Hu and co-workers disclosed a new molecule
385 UF146 as an inhibitor of the UHRF1-SRA/Sin3A-associated protein 30 (SAP30) interaction,
386 preventing the transcription of MXD4 affecting the self-renewal of leukemia initiation cells (LICs)⁵⁶.
387 Although UF146 formally qualifies as a PAINS^{57,58} due to the presence of the quinone moiety, it is
388 structurally related to UM63 and mitoxantrone, which corroborates the screening strategy adopted in
389 this work for the identification of new chemotypes of UHRF1 inhibitors.

390 Taken together, our data indicate that AMSA2 and MPB7 are promising UHRF1 inhibitors that inhibit
391 the base flipping activity of the SRA domain and prevent DNMT1 recruitment on the replication foci.
392 The two compounds also decreased the DNA methylation level, which compromises the viability of

393 the treated cells. Cancer cells were found to be more sensitive than normal cells, likely as a
394 consequence of their higher UHRF1 expression levels. The investigation of the cellular mechanisms
395 and anticancer activities of the two compounds is currently in progress.

396

397 **Materials and Methods**

398 **Chemicals, oligonucleotides and protein**

399 All tested compounds were purchased from Aldrich Market Select (Milwaukee, Wisconsin, USA)
400 and MolPort (Riga, Latvia). The MPB7 purity provided by the vendor (Toronto Research Chemicals,
401 $\geq 98\%$) and the AMSA2 purity determined in our lab by HPLC were $> 95\%$ (**Fig. S6**). Both
402 compounds were initially dissolved in 99% pure DMSO (Sigma Aldrich) as stock solutions, aliquoted
403 (avoiding freeze-thaw cycles) and stored at $-20\text{ }^{\circ}\text{C}$ until further use. 5-azacitidine ($\geq 98\%$, HPLC)
404 was purchased from Sigma Aldrich. DNA duplexes were prepared by annealing equal molar amounts
405 of complementary oligonucleotides in a PCR thermocycler (BIO-RAD T100TM) using 20 mM
406 phosphate buffer pH 7.5, 150 mM NaCl. Unlabeled 5'-GGGCCmCGCAGGG-3' and complementary
407 5'-CCCTGCGGGCCC-3' oligonucleotides were purchased from IBA GmbH Nucleic Acids Product
408 Supply (Germany) in a HPLC-purified form. Labelled 5'-GGGCCmCthGCAGGG-3' oligonucleotide
409 with thienoguanosine (thG) at position 7 was purchased from TriLink Biotechnologies (USA). The
410 5'-GGGCCmCGCAGGG-3' sequence labelled with 6-Carboxyfluorescein (6FAM) at the 5' end was
411 purchased from Eurogentec (Belgium). The SRA domain (residues 408-643) of UHRF1 was
412 expressed and purified as described previously⁸⁵.

413

414 **Absorption Spectroscopy**

415 Absorption spectra were recorded on a Cary 4000 UV-visible spectrophotometer (Varian) using
416 quartz cuvettes (Hellma Analytics) of 1 cm optical path length. Absorption coefficients of 112,950
417 $\text{M}^{-1}\text{cm}^{-1}$ and 97,300 $\text{M}^{-1}\text{cm}^{-1}$ at 260 nm were used for the single strand non-labelled 5'-

418 GGGCCmCGCAGGG-3' and complementary 5'-CCCTGCGGGCCC-3' sequences, respectively.
419 Absorption coefficients at 260 nm of 103,000 M⁻¹cm⁻¹ and 131,800 M⁻¹cm⁻¹ were used for the single
420 strand thG-labelled 5'-GGGCCmCthGCAGGG-3' and 6FAM-labelled 5'-GGGCCmCGCAGGG-3'
421 sequences, respectively. Absorption coefficients at 260 nm of 183,340 M⁻¹cm⁻¹ and 209,900 M⁻¹cm⁻¹
422 were used for the thG-labelled and 6FAM-labelled duplexes, respectively. For SRA, an absorption
423 coefficient of 43,890 M⁻¹cm⁻¹ at 280 nm was used. All the experiments were performed at 20°C in
424 20 mM phosphate buffer pH 7.5, 50 mM NaCl, 2.5 mM TCEP and PEG 0.05% to avoid protein
425 adsorption to the quartz cuvette⁶⁶.

426

427 **Steady-State Fluorescence Spectroscopy**

428 Fluorescence spectra were collected at 20 °C on a FluoroLog spectrofluorometer (Horiba) equipped
429 with a thermostated cell compartment. For thG-labelled duplexes, excitation wavelengths ranging
430 from 320 to 360 nm were used. For ethidium bromide, excitation was at 526 nm, slits 5 nm. All the
431 spectra were corrected for lamp fluctuations and instrumental wavelength-dependent bias as well as
432 for the fluorescence of the buffer and the compounds selected by *in silico* screening.

433 To determine whether positive hits are able to dissociate the complexes of SRA with HM duplex, we
434 performed fluorescence anisotropy measurements with 6FAM-labelled HM duplexes. Increasing
435 concentrations of the hits were added to the SRA/HM duplex complex. For each addition, the
436 fluorescence anisotropy of the complex was monitored with a FluoroLog spectrofluorometer (Horiba)
437 in T-format. Anisotropy values were the average of 10 measurements per data point. Excitation was
438 at 495 nm, slits 2 nm, and emission was at 517 nm, slits 4 nm.

439

440 **Molecular modelling**

441 The Aldrich Market Select and MolPort commercial libraries of compounds containing 8'512'248
442 and 7'591'844 entries, respectively, at the time of this study (May 2019), were downloaded in
443 SMILES format. Filtration was performed with the FILTER application implemented in OMEGA

444 (version 2.5.1.4) from OpenEye⁸⁶ (OpenEye Scientific Software, Santa FE, NM.
445 <http://www.eyesopen.com>) using the SMARTS strings corresponding to the scaffold of UM63 and
446 its substructures. Two SMARTS strings were drawn based on UM63 full structure, while 6 SMARTS
447 strings were drawn based on the possible UM63's substructures. Filtration of the initial libraries
448 against the SMARTS strings led to 1'352'537 and 3'746'065 molecules from Aldrich Market Select
449 and MolPort, respectively, whose protonation state was assigned by QUACPAC from OpenEye
450 (version 2.5.1.4) (OpenEye Scientific Software, Santa FE, NM. <http://www.eyesopen.com>).
451 Conformational analysis was performed with OMEGA (version 2.5.1.4) keeping all default settings
452 and allowing the storage of up to 600 conformers per molecule. The crystallographic structure of the
453 SRA domain of UHRF1 bound to hemi-methylated DNA (PDB_ID: 3CLZ)²⁴ was used as a rigid
454 receptor in molecular docking simulations after removing DNA and water molecules²⁸. Docking-
455 based virtual screening was performed with FRED from OpenEye (version 3.0.1) using default
456 settings and retaining only the best pose of each docked molecule. At the end of this process, 150
457 potential hits were selected for further visual inspection, based on their score. Finally, coupling visual
458 inspection with the analysis of the score led to the prioritization of 64 molecules for experimental
459 testing.

460 Subsequent in-depth docking investigation on AMSA2 and MPB7 was carried out with FRED, using
461 the highest docking resolution settings and retaining 10 poses in order to explore the AMSA2 and
462 MPB7 binding mode with a higher precision compared to virtual screening settings.

463

464 ***In vitro* fluorescence-based base flipping assay**

465 The first round of *in vitro* screening was performed by using a fluorescence-based base flipping assay
466 with 0.5 μM of ³H-labelled HM DNA and 1.5 μM of SRA domain in 20 mM phosphate buffer at pH
467 7.5, 50 mM NaCl, 2.5 mM TCEP, PEG 20.000 0.05%. Before the screening, each compound was
468 checked for its fluorescence using ³H excitation range (320 to 360 nm). If the compound showed
469 fluorescence, its emission spectrum in buffer was recorded for subtraction. For the first round of

470 screening, the compounds were tested at 10 μ M. Absorbance measurements were collected in parallel
471 to check for aggregation. The inhibition percentage of the SRA-induced base flipping for a given
472 compound was determined using:

$$473 \quad \%inhibition = \frac{F.I.(dsDNA+SRA) - F.I.(dsDNA+SRA+inhibitor)}{F.I.(dsDNA+SRA) - F.I.(dsDNA)} * 100 \quad (1)$$

474 where $F.I.(dsDNA)$, $F.I.(dsDNA+SRA)$, and $F.I.(dsDNA+SRA+inhibitor)$, correspond to the fluorescence intensity of
475 thG-labelled HM duplex alone, in the presence of SRA, and in the presence of both SRA and inhibitor,
476 respectively.

477 Compounds with an inhibitory effect > 30% at 10 μ M were selected and their half maximal inhibitory
478 concentration (IC_{50}) was determined on the same assay using 2 μ M of thG-labelled HM DNA and 3
479 μ M SRA. The compounds were added to this mixture at concentrations ranging from 1 to 40 μ M.
480 Absorbance measurements were collected in parallel to check for aggregation. The percentage of
481 inhibition was determined by equation (1) and the resulting dose-response curve was fitted using:

$$482 \quad \%inhibition = I_0 + \frac{I_f - I_0}{1 + 10^{\{(\log(IC_{50}) - C) * p\}}} \quad (2)$$

483 where I_0 and I_f correspond to the percentage of inhibition in the absence and at saturating
484 concentration of the hit, respectively. C is the concentration of the hit, and p is the Hill coefficient⁸⁷.

485

486 **Cell culture**

487 HeLa cells (ATCC, CCL-2 Amp, HeLa; Cervical Adenocarcinoma; Human), A375 (ATCC, CRL-
488 1619 A-375; Malignant Melanoma; Human), T47D (ATCC, CRL-2865 T47D-KBluc; Ductal
489 Carcinoma; Human) and BJ (ATCC, CRL-2522 BJ; Normal fibroblast; Human) were grown in
490 DMEM (Dulbecco's Modified Eagle's Medium) or RPMI (Roswell Park Memorial Institute) 1640
491 culture media, supplemented with 10% FBS (fetal bovine serum) and penicillin (100 U/mL) and
492 streptomycin (100 U/mL) (Invitrogen Corporation Pontoise, France). Cells were grown at 37 °C with
493 5% CO₂. HeLa, A375 and T47D were purchased from ATCC. BJ cells were kindly gifted from Dr.
494 Christian Muller (Faculty of Pharmacy, Illkirch, France).

495

496 **Cell proliferation and viability**

497 HeLa, A375, T47D, and BJ cells were seeded in 96-well plate at a density of 5×10^3 cells/well, kept
498 for 24 h in DMEM medium supplemented with 10% FBS to allow cell attachment and then incubated
499 for additional 48 h in the presence of the selected compounds at different concentrations, along with
500 the control sample, in the absence of any compound. Each concentration was tested in hexaplicate.
501 One hundred microliters of tetrazolium dye 3-(4,5-dimethylthiazol-2-yl)-2,5-diphenyltetrazolium
502 bromide (MTT) reagent (1 mg/mL) were added to each well. Then, cells were incubated for 4 h at 37
503 °C. The medium was discarded and 50 μ L of dimethylsulfoxide (DMSO) were added to each well to
504 dissolve formazan salts. Plates were gently mixed until the dissolution of the formazan crystals. Then,
505 absorbance at 540 nm was measured on a plate reader Xenius (SAFAS, Monaco) in a single point
506 format, with bandwidth 2 nm, integration time 1 s. Four measurements were performed for each well,
507 with a shift of 0.2 mm between two measurements and the average value was calculated. All values
508 were corrected by subtracting the absorbance of the cell culture medium alone. The percentage of
509 inhibition for each compound was calculated using:

510
$$\%inhibition = \frac{(Treated\ Cells - Untreated\ cells)}{Untreated\ Cells} * 100 \quad (3)$$

511

512 **Plasmids and transient transfection**

513 UHRF1-mCherry plasmid (tag: mCherry, resistance: ampicillin, vector backbone: pCMV-mCherry,
514 promoter: CMV) and eGFP-DNMT1 plasmid (tag: eGFP at N-terminal, resistance: kanamycin, vector
515 backbone: pEGFP-C2, promoter: CMV) were used. To transfect the selected plasmids in HeLa cells,
516 jetPEI™ (Life Technologies, Saint Aubin, France) was used following the manufacturer's protocol.

517

518 **Antibodies**

519 Primary antibodies used in this study include rabbit polyclonal anti-DNMT1 (Invitrogen, PA5-
520 30581), mouse monoclonal anti-UHRF1 (engineered as described previously³³), rabbit monoclonal
521 anti-GAPDH (Merck Millipore MAB374) and mouse monoclonal anti-5-methylcytosine (Active
522 Motif 39649). Polyclonal anti-Mouse (HRP Conjugate Promega France, W4021), polyclonal anti-
523 Rabbit (HRP Conjugate Promega France, W4011) and polyclonal anti-Mouse (H+L) (Cross-adsorbed
524 alexa fluor 488, Invitrogen A-11001) were used as secondary antibodies.

525

526 **Western Blots**

527 HeLa, A375, T47D and BJ cells were seeded at a final density of 7.5×10^4 cells/mL in a 6-well plate
528 and kept for 24 h in DMEM medium supplemented with 10% FBS to allow cell attachment. Cells
529 were then incubated for 48 h with AMSA2 (10 and 50 μ M) and MPB7 (10 and 30 μ M) along with
530 untreated cells. Then, cells were harvested, washed with PBS and then sonicated in ice cold lysis
531 buffer (10 mM Tris-HCl pH 7.5, 150 mM NaCl, 1 mM EDTA and 1% NP40) supplemented with
532 cOmplete™ Protease Inhibitor Cocktail (PIC) (Roche Germany, 11836170001). Total proteins were
533 quantified by Bradford protein assay. Protein samples were denatured by heating at 95°C for 5 min
534 in Laemmli sample buffer (Bio-Rad, 1610747) freshly supplemented with β -mercaptoethanol. 40 μ g
535 of proteins from each sample were loaded to SDS-PAGE (10%). Electrophoresis was performed in
536 Tris-Glycine migration buffer (Tris 25 mM, Glycine 192 mM, SDS 0.1%, pH 8.8) by using a minigel
537 system (Bio-Rad). After migration, proteins were transferred to PVDF (polyvinylidene difluoride)
538 membranes, previously activated by methanol in transfer buffer (Tris 25 mM, Glycine 192 mM and
539 30% methanol, pH 6.8). PVDF membranes were blocked with Superblock T20 blocking buffer
540 (Thermo-scientific-37516) for 1 h at RT. After blocking, membranes were incubated overnight with
541 the corresponding primary antibodies at 4°C. Membranes were then washed thrice with TBST buffer
542 before being incubated with secondary antibodies for 1 h at RT. After further washing in TBST,
543 signals were visualized with an Image Quant LAS 4000 apparatus (GE Healthcare Life Sciences,
544 USA) using chemiluminescent ECL system (Clarity™ ECL western blotting substrate, Bio-Rad,

545 France, 170-5060). The images were captured with the Image Studio Lite (Li-Core Biosciences,
546 USA) software and further processed with ImageJ software. The band signal for each sample was
547 normalized with the corresponding GAPDH signal using the following formula:

$$548 \quad \text{Normalized signal} = \frac{X/N.C.}{GAPDH,N.C./X,GAPDH} \quad (4)$$

549 where X is the band signal; $N.C.$ is the band signal of the negative control (untreated cells); $GAPDH$,
550 $N.C.$ is the band signal of GAPDH for untreated cells; X , $GAPDH$ is the corresponding GAPDH band
551 signal of treated cells.

552

553 **Confocal microscopy**

554 To assess UHRF1 and DNMT1 co-localization, HeLa cells were seeded in 6-well plate on a coverslip
555 at a density of 5×10^4 cells/mL and kept for 24 h in DMEM medium supplemented with 10% FBS to
556 allow cell attachment. Then, cells were co-transfected with eGFP-DNMT1 and UHRF1-mCherry
557 plasmids and incubated for 24 h with AMSA2 50 μ M or MPB7 30 μ M, along with the control, in the
558 absence of any compound. Cells were fixed with 4% paraformaldehyde for 15 min and then,
559 permeabilized with 0.5% Triton X-100 for 20 min at RT. Cells were then incubated with Hoechst at
560 2 μ g/mL, to stain nuclei. Cells in S phase were detected by using the Click-iT™ Plus EdU Cell
561 Proliferation Kit for Imaging, with Alexa Fluor™ 647 dye (Thermo Fisher Scientific USA C10640)
562 according to the manufacturer's protocol. All samples were imaged with a Leica TCS SPE confocal
563 microscope equipped with an HXC PL APO63 \times /1.40 OIL CS oil immersion objective. Hoechst,
564 eGFP-DNMT1, UHRF1-mCherry and EdU-Alexa 647 were excited at 405 nm (laser 10 mW), 488
565 nm (laser 25 mW), 561 nm (laser 10 mW) and 635 nm (laser 18 mW), respectively. The detection
566 range for the four dyes was 430-480 nm, 493-548 nm, 571-683 nm, 645-754 nm, respectively. All
567 the images were processed with the ImageJ software. Co-localization of tagged proteins was
568 evaluated through Pearson correlation coefficient (PCC), obtained with the "Squassh" plugin of
569 ImageJ⁸⁸.

570 In order to quantify the global methylation level, HeLa cells were seeded in 6-well plate on a coverslip
571 at a density of 7.5×10^4 cells/mL, kept for 24 h in DMEM media supplemented with 10% FBS to allow
572 cell attachment and then incubated for 48 h with AMSA2 (10 and 50 μ M) or MPB7 (10 and 30 μ M),
573 along with the control sample or in the absence of any compound. Cells were fixed with 4%
574 paraformaldehyde for 15 min and then, permeabilized with 0.5% Triton X-100 for 20 min at RT.
575 Next, DNA was denatured using 4 M HCl for 20 minutes at RT, which was then removed and
576 neutralized with 100 mM Tris HCl pH 8.8 for 10 min at RT. Subsequently, samples were blocked
577 with Superblock T20 blocking buffer for 1 h at RT and then incubated with primary antibody against
578 5mC o/n at 4 °C. After washing three times with PBS 1% BSA supplemented with 0.05% Tween,
579 anti-goat secondary antibody coupled to Alexa Fluor 488 was added. All samples were imaged with
580 a Leica TCS SPE confocal microscope equipped with a 20X air (0.7 NA) immersion lens objective.
581 Then, images were further processed with ImageJ software and global DNA methylation signal was
582 calculated as the mean fluorescence in the field per number of particles captured in a single image
583 without zoom⁸⁹.

584

585 **DNA global methylation inhibition assay**

586 HeLa cells were seeded in 6-well plate at a density of 7.5×10^4 cells/mL, kept for 24 h in DMEM
587 media supplemented with 10% FBS to allow cell attachment and then incubated for 48 h with AMSA2
588 (10 and 50 μ M), MPB7 (10 and 30 μ M) and 5-azacytidine (100 μ M) (Sigma-Aldrich), along with
589 untreated cells. QIAamp® DNA Kit (QIAGEN, Catalog no. 51304) was used for DNA purification.
590 Enzymatic digestion of DNA by methylation sensitive and insensitive enzymes, *HpaII* and *MspI*
591 respectively, was assessed on 1% agarose gel in TBE buffer. The enzymatic digestion was performed
592 on 0.45 μ g of DNA extracted from treated or untreated cells. Sample preparation and enzymatic
593 reactions were performed following the protocol of the EpiJET DNA Methylation Analysis Kit
594 (*MspI/HpaII*) (ThermoFisher, Catalog no. K1441).

595

596 **Statistical analysis**

597 All experiments were repeated at least three times and the obtained data were statistically compared
598 by one-way ANOVA with post-hoc Bonferroni test using GraphPad-Prism (version 5.04) software.

599

600 **Supporting Information**

- 601 • Aldrich Market Select (AMS) structures list.
- 602 • MolPort (MP) structures list.
- 603 • Results first round of *in vitro* screening.
- 604 • Results second round of *in vitro* screening.
- 605 • UM63 data from Zaayter et al, 2019.
- 606 • Anisotropy data for AMSA2 and MPB7.
- 607 • AMSA2 and MPB7 binding mode overlapping with 5mC
- 608 • Purity data and instrument method.

609

610 **Authorship contributions**

611 Conceptualization, supervision and funding acquisition: Mousli M., Mori M., Mély Y.; Data
612 acquisition and discussion: Ciaco S., Mazzoleni V., Javed A., Mousli M., Mori M., Mély Y.; Protein
613 production and purification: Eiler S., Ruff M.; Writing - original draft: Ciaco S., Mazzoleni V.;
614 Writing - review and editing: Ciaco S., Mazzoleni V., Javed A., Mousli M., Mori M., Mély Y.

615 All authors have read and agreed to the published version of the manuscript.

616

617 **Declaration of competing interest**

618 The authors declare that they have no known competing financial interests or personal relationships
619 that could have appeared to influence the work reported in this paper.

620

621 **Acknowledgements**

622 We thank T. Lequeu for his technical help in preparing SRA and N. Humbert for his help in checking
623 AMSA2 purity. This work was supported by the Agence Nationale de la Recherche (ANR blanc
624 SMFLUONA), the Labex NIE, the Région Grand-Est (EpiRNA project) and the Centre National pour
625 la Recherche Scientifique (CNRS). Y.M. is grateful to the Institut Universitaire de France (IUF) for
626 support and providing additional time to be dedicated to research. S.C. was supported by a fellowship
627 from Region Grand Est. A.J. was supported by a fellowship from HEC Pakistan. M.M. (University
628 of Siena) wish to thank the OpenEye Free Academic Licensing Program for providing a free academic
629 license for molecular modeling and chemoinformatics software. Imaging was supported by the
630 Imaging Center PIQ-QuESt (<https://piq.unistra.fr/>).

631

632 **References**

- 633 1. Sung H, Ferlay J, Siegel RL, et al. Global Cancer Statistics 2020: GLOBOCAN Estimates of
634 Incidence and Mortality Worldwide for 36 Cancers in 185 Countries. *CA Cancer J Clin.*
635 2021;71(3):209-249. doi:10.3322/caac.21660
- 636 2. Ferlay J, Colombet M, Soerjomataram I, et al. Cancer statistics for the year 2020: An
637 overview. *Int J Cancer.* Published online April 5, 2021. doi:10.1002/ijc.33588
- 638 3. Oberst A, Rossi M, Salomoni P, et al. Regulation of the p73 protein stability and
639 degradation. *Biochem Biophys Res Commun.* 2005;331(3):707-712. doi:10.1016/j.bbrc.2005.03.158
- 640 4. Yang CS, Yu C, Chuang HC, et al. FBW2 Targets GCMa to the Ubiquitin-Proteasome
641 Degradation System *. *Journal of Biological Chemistry.* 2005;280(11):10083-10090.
642 doi:10.1074/jbc.M413986200
- 643 5. Esteller M. Epigenetic gene silencing in cancer: the DNA hypermethylation. *Hum Mol*
644 *Genet.* 2007;16 Spec No 1:R50-59. doi:10.1093/hmg/ddm018
- 645 6. Esteller M. Cancer epigenomics: DNA methylomes and histone-modification maps. *Nat Rev*
646 *Genet.* 2007;8(4):286-298. doi:10.1038/nrg2005
- 647 7. Kurdistani SK. Histone modifications as markers of cancer prognosis: a cellular view. *Br J*
648 *Cancer.* 2007;97(1):1-5. doi:10.1038/sj.bjc.6603844
- 649 8. Baylin SB, Jones PA. Epigenetic Determinants of Cancer. *Cold Spring Harb Perspect Biol.*
650 2016;8(9). doi:10.1101/cshperspect.a019505
- 651 9. Feinberg AP, Ohlsson R, Henikoff S. The epigenetic progenitor origin of human cancer. *Nat*
652 *Rev Genet.* 2006;7(1):21-33. doi:10.1038/nrg1748
- 653 10. Ashraf W, Ibrahim A, Alhosin M, et al. The epigenetic integrator UHRF1: on the road to
654 become a universal biomarker for cancer. *Oncotarget.* 2017;8(31):51946-51962.
655 doi:10.18632/oncotarget.17393

- 656 11. Boukhari A, Alhosin M, Bronner C, et al. CD47 activation-induced UHRF1 over-expression
657 is associated with silencing of tumor suppressor gene p16INK4A in glioblastoma cells. *Anticancer*
658 *Res.* 2015;35(1):149-157.
- 659 12. Jeanblanc M, Mousli M, Hopfner R, et al. The retinoblastoma gene and its product are
660 targeted by ICBP90: a key mechanism in the G1/S transition during the cell cycle. *Oncogene.*
661 2005;24(49):7337-7345. doi:10.1038/sj.onc.1208878
- 662 13. Unoki M, Brunet J, Mousli M. Drug discovery targeting epigenetic codes: the great potential
663 of UHRF1, which links DNA methylation and histone modifications, as a drug target in cancers and
664 toxoplasmosis. *Biochem Pharmacol.* 2009;78(10):1279-1288. doi:10.1016/j.bcp.2009.05.035
- 665 14. Wang F, Yang YZ, Shi CZ, et al. UHRF1 promotes cell growth and metastasis through
666 repression of p16(ink^{4a}) in colorectal cancer. *Ann Surg Oncol.* 2012;19(8):2753-2762.
667 doi:10.1245/s10434-011-2194-1
- 668 15. Jones PA, Issa JPJ, Baylin S. Targeting the cancer epigenome for therapy. *Nat Rev Genet.*
669 2016;17(10):630-641. doi:10.1038/nrg.2016.93
- 670 16. Alhosin M, Sharif T, Mousli M, et al. Down-regulation of UHRF1, associated with re-
671 expression of tumor suppressor genes, is a common feature of natural compounds exhibiting anti-
672 cancer properties. *J Exp Clin Cancer Res.* 2011;30(1):41. doi:10.1186/1756-9966-30-41
- 673 17. Unoki M, Nishidate T, Nakamura Y. ICBP90, an E2F-1 target, recruits HDAC1 and binds to
674 methyl-CpG through its SRA domain. *Oncogene.* 2004;23(46):7601-7610.
675 doi:10.1038/sj.onc.1208053
- 676 18. Bronner C, Krifa M, Mousli M. Increasing role of UHRF1 in the reading and inheritance of
677 the epigenetic code as well as in tumorigenesis. *Biochemical Pharmacology.* 2013;86(12):1643-
678 1649. doi:10.1016/j.bcp.2013.10.002
- 679 19. Achour M, Fuhrmann G, Alhosin M, et al. UHRF1 recruits the histone acetyltransferase
680 Tip60 and controls its expression and activity. *Biochem Biophys Res Commun.* 2009;390(3):523-
681 528. doi:10.1016/j.bbrc.2009.09.131
- 682 20. Kim JK, Estève PO, Jacobsen SE, Pradhan S. UHRF1 binds G9a and participates in p21
683 transcriptional regulation in mammalian cells. *Nucleic Acids Res.* 2009;37(2):493-505.
684 doi:10.1093/nar/gkn961
- 685 21. Sharif J, Muto M, Takebayashi S ichiro, et al. The SRA protein Np95 mediates epigenetic
686 inheritance by recruiting Dnmt1 to methylated DNA. *Nature.* 2007;450(7171):908-912.
687 doi:10.1038/nature06397
- 688 22. Bostick M, Kim JK, Estève PO, Clark A, Pradhan S, Jacobsen SE. UHRF1 plays a role in
689 maintaining DNA methylation in mammalian cells. *Science.* 2007;317(5845):1760-1764.
690 doi:10.1126/science.1147939
- 691 23. Arita K, Ariyoshi M, Tochio H, Nakamura Y, Shirakawa M. Recognition of hemi-
692 methylated DNA by the SRA protein UHRF1 by a base-flipping mechanism. *Nature.*
693 2008;455(7214):818-821. doi:10.1038/nature07249
- 694 24. Avvakumov GV, Walker JR, Xue S, et al. Structural basis for recognition of hemi-
695 methylated DNA by the SRA domain of human UHRF1. *Nature.* 2008;455(7214):822-825.
696 doi:10.1038/nature07273
- 697 25. Liu X, Gao Q, Li P, et al. UHRF1 targets DNMT1 for DNA methylation through
698 cooperative binding of hemi-methylated DNA and methylated H3K9. *Nat Commun.* 2013;4:1563.
699 doi:10.1038/ncomms2562
- 700 26. Arita K, Isogai S, Oda T, et al. Recognition of modification status on a histone H3 tail by
701 linked histone reader modules of the epigenetic regulator UHRF1. *Proceedings of the National*
702 *Academy of Sciences.* 2012;109(32):12950-12955. doi:10.1073/pnas.1203701109
- 703 27. Cheng J, Yang Y, Fang J, et al. Structural Insight into Coordinated Recognition of
704 Trimethylated Histone H3 Lysine 9 (H3K9me₃) by the Plant Homeodomain (PHD) and Tandem
705 Tudor Domain (TTD) of UHRF1 (Ubiquitin-like, Containing PHD and RING Finger Domains, 1)
706 Protein. *J Biol Chem.* 2013;288(2):1329-1339. doi:10.1074/jbc.M112.415398

- 707 28. Fang J, Cheng J, Wang J, et al. Hemi-methylated DNA opens a closed conformation of
708 UHRF1 to facilitate its histone recognition. *Nat Commun.* 2016;7:11197.
709 doi:10.1038/ncomms11197
- 710 29. Nishiyama A, Yamaguchi L, Sharif J, et al. Uhrf1-dependent H3K23 ubiquitylation couples
711 maintenance DNA methylation and replication. *Nature.* 2013;502(7470):249-253.
712 doi:10.1038/nature12488
- 713 30. Vaughan RM, Rothbart SB, Dickson BM. The finger loop of the SRA domain in the E3
714 ligase UHRF1 is a regulator of ubiquitin targeting and is required for the maintenance of DNA
715 methylation. *J Biol Chem.* 2019;294(43):15724-15732. doi:10.1074/jbc.RA119.010160
- 716 31. Hu L, Li Z, Wang P, Lin Y, Xu Y. Crystal structure of PHD domain of UHRF1 and insights
717 into recognition of unmodified histone H3 arginine residue 2. *Cell Res.* 2011;21(9):1374-1378.
718 doi:10.1038/cr.2011.124
- 719 32. Hashimoto H, Horton JR, Zhang X, Bostick M, Jacobsen SE, Cheng X. The SRA domain of
720 UHRF1 flips 5-methylcytosine out of the DNA helix. *Nature.* 2008;455(7214):826-829.
721 doi:10.1038/nature07280
- 722 33. Hopfner R, Mousli M, Jeltsch JM, et al. ICBP90, a novel human CCAAT binding protein,
723 involved in the regulation of topoisomerase IIalpha expression. *Cancer Res.* 2000;60(1):121-128.
- 724 34. Mousli M, Hopfner R, Abbady AQ, et al. ICBP90 belongs to a new family of proteins with
725 an expression that is deregulated in cancer cells. *Br J Cancer.* 2003;89(1):120-127.
726 doi:10.1038/sj.bjc.6601068
- 727 35. Alhosin M, Omran Z, Zamzami MA, et al. Signalling pathways in UHRF1-dependent
728 regulation of tumor suppressor genes in cancer. *J Exp Clin Cancer Res.* 2016;35:174.
729 doi:10.1186/s13046-016-0453-5
- 730 36. Jin W, Chen L, Chen Y, et al. UHRF1 is associated with epigenetic silencing of BRCA1 in
731 sporadic breast cancer. *Breast Cancer Res Treat.* 2010;123(2):359-373. doi:10.1007/s10549-009-
732 0652-2
- 733 37. Daskalos A, Oleksiewicz U, Filia A, et al. UHRF1-mediated tumor suppressor gene
734 inactivation in nonsmall cell lung cancer. *Cancer.* 2011;117(5):1027-1037. doi:10.1002/cncr.25531
- 735 38. Krifa M, Alhosin M, Muller CD, et al. Limoniastrum guyonianum aqueous gall extract
736 induces apoptosis in human cervical cancer cells involving p16INK4A re-expression related to
737 UHRF1 and DNMT1 down-regulation. *J Exp Clin Cancer Res.* 2013;32(1):30. doi:10.1186/1756-
738 9966-32-30
- 739 39. Matsushita R, Yoshino H, Enokida H, et al. Regulation of UHRF1 by dual-strand tumor-
740 suppressor microRNA-145 (miR-145-5p and miR-145-3p): inhibition of bladder cancer cell
741 aggressiveness. *Oncotarget.* 2016;7(19):28460-28487. doi:10.18632/oncotarget.8668
- 742 40. Ashraf W, Ahmad T, Almalki NAR, et al. Tannin extract from maritime pine bark exhibits
743 anticancer properties by targeting the epigenetic UHRF1/DNMT1 tandem leading to the re-
744 expression of TP73. *Food Funct.* Published online December 13, 2021. doi:10.1039/d1fo01484f
- 745 41. Yang X, Lay F, Han H, Jones PA. Targeting DNA methylation for epigenetic therapy.
746 *Trends Pharmacol Sci.* 2010;31(11):536-546. doi:10.1016/j.tips.2010.08.001
- 747 42. Thurn KT, Thomas S, Moore A, Munster PN. Rational therapeutic combinations with
748 histone deacetylase inhibitors for the treatment of cancer. *Future Oncol.* 2011;7(2):263-283.
749 doi:10.2217/fon.11.2
- 750 43. Kantarjian H, Issa JPJ, Rosenfeld CS, et al. Decitabine improves patient outcomes in
751 myelodysplastic syndromes: results of a phase III randomized study. *Cancer.* 2006;106(8):1794-
752 1803. doi:10.1002/cncr.21792
- 753 44. Chuang JC, Yoo CB, Kwan JM, et al. Comparison of biological effects of non-nucleoside
754 DNA methylation inhibitors versus 5-aza-2'-deoxycytidine. *Mol Cancer Ther.* 2005;4(10):1515-
755 1520. doi:10.1158/1535-7163.MCT-05-0172
- 756 45. Foulks JM, Parnell KM, Nix RN, et al. Epigenetic drug discovery: targeting DNA
757 methyltransferases. *J Biomol Screen.* 2012;17(1):2-17. doi:10.1177/1087057111421212

- 758 46. Jung Y, Park J, Kim TY, et al. Potential advantages of DNA methyltransferase 1 (DNMT1)-
759 targeted inhibition for cancer therapy. *J Mol Med (Berl)*. 2007;85(10):1137-1148.
760 doi:10.1007/s00109-007-0216-z
- 761 47. Pali SS, Van Emburgh BO, Sankpal UT, Brown KD, Robertson KD. DNA methylation
762 inhibitor 5-Aza-2'-deoxycytidine induces reversible genome-wide DNA damage that is distinctly
763 influenced by DNA methyltransferases 1 and 3B. *Mol Cell Biol*. 2008;28(2):752-771.
764 doi:10.1128/MCB.01799-07
- 765 48. Bronner C, Achour M, Arima Y, Chataigneau T, Saya H, Schini-Kerth VB. The UHRF
766 family: oncogenes that are drugable targets for cancer therapy in the near future? *Pharmacol Ther*.
767 2007;115(3):419-434. doi:10.1016/j.pharmthera.2007.06.003
- 768 49. Unoki M. Current and potential anticancer drugs targeting members of the UHRF1 complex
769 including epigenetic modifiers. *Recent Pat Anticancer Drug Discov*. 2011;6(1):116-130.
770 doi:10.2174/157489211793980024
- 771 50. Myriantopoulos V, Cartron PF, Liutkevičiūtė Z, et al. Tandem virtual screening targeting
772 the SRA domain of UHRF1 identifies a novel chemical tool modulating DNA methylation. *Eur J*
773 *Med Chem*. 2016;114:390-396. doi:10.1016/j.ejmech.2016.02.043
- 774 51. Houliston RS, Lemak A, Iqbal A, et al. Conformational dynamics of the TTD-PHD histone
775 reader module of the UHRF1 epigenetic regulator reveals multiple histone-binding states, allosteric
776 regulation, and druggability. *J Biol Chem*. 2017;292(51):20947-20959.
777 doi:10.1074/jbc.M117.799700
- 778 52. Parker BS, Cutts SM, Nudelman A, Rephaeli A, Phillips DR, Sukumar S. Mitoxantrone
779 mediates demethylation and reexpression of cyclin d2, estrogen receptor and 14.3.3sigma in breast
780 cancer cells. *Cancer Biol Ther*. 2003;2(3):259-263. doi:10.4161/cbt.2.3.364
- 781 53. Wyhs N, Walker D, Giovinazzo H, Yegnasubramanian S, Nelson WG. Time-Resolved
782 Fluorescence Resonance Energy Transfer Assay for Discovery of Small-Molecule Inhibitors of
783 Methyl-CpG Binding Domain Protein 2. *J Biomol Screen*. 2014;19(7):1060-1069.
784 doi:10.1177/1087057114526433
- 785 54. Giovinazzo H, Walker D, Wyhs N, et al. A high-throughput screen of pharmacologically
786 active compounds for inhibitors of UHRF1 reveals epigenetic activity of anthracycline derivative
787 chemotherapeutic drugs. *Oncotarget*. 2019;10(32):3040-3050. doi:10.18632/oncotarget.26889
- 788 55. Zaayter L, Mori M, Ahmad T, et al. A Molecular Tool Targeting the Base-Flipping Activity
789 of Human UHRF1. *Chem Eur J*. 2019;25(58):13363-13375. doi:10.1002/chem.201902605
- 790 56. Hu CL, Chen BY, Li Z, et al. Targeting UHRF1-SAP30-MXD4 axis for leukemia initiating
791 cell eradication in myeloid leukemia. *Cell Res*. Published online October 27, 2022:1-19.
792 doi:10.1038/s41422-022-00735-6
- 793 57. Baell JB, Holloway GA. New substructure filters for removal of pan assay interference
794 compounds (PAINS) from screening libraries and for their exclusion in bioassays. *J Med Chem*.
795 2010;53(7):2719-2740. doi:10.1021/jm901137j
- 796 58. Baell J, Walters MA. Chemistry: Chemical con artists foil drug discovery. *Nature*.
797 2014;513(7519):481-483. doi:10.1038/513481a
- 798 59. McGann M. FRED pose prediction and virtual screening accuracy. *J Chem Inf Model*.
799 2011;51(3):578-596. doi:10.1021/ci100436p
- 800 60. Stahl M, Mauser H. Database clustering with a combination of fingerprint and maximum
801 common substructure methods. *J Chem Inf Model*. 2005;45(3):542-548. doi:10.1021/ci050011h
- 802 61. Mori M, Tottone L, Quaglio D, et al. Identification of a novel chalcone derivative that
803 inhibits Notch signaling in T-cell acute lymphoblastic leukemia. *Sci Rep*. 2017;7(1):2213.
804 doi:10.1038/s41598-017-02316-9
- 805 62. Mori M, Kovalenko L, Malancona S, et al. Structure-Based Identification of HIV-1
806 Nucleocapsid Protein Inhibitors Active against Wild-Type and Drug-Resistant HIV-1 Strains. *ACS*
807 *Chem Biol*. 2018;13(1):253-266. doi:10.1021/acscchembio.7b00907
- 808 63. Shin D, Sinkeldam RW, Tor Y. Emissive RNA Alphabet. *J Am Chem Soc*.

809 2011;133(38):14912-14915. doi:10.1021/ja206095a
810 64. Sholokh M, Sharma R, Shin D, et al. Conquering 2-Aminopurine's Deficiencies: Highly
811 Emissive Isomorphous Guanosine Surrogate Faithfully Monitors Guanosine Conformation and
812 Dynamics in DNA. *J Am Chem Soc.* 2015;137(9):3185-3188. doi:10.1021/ja513107r
813 65. Park S, Otomo H, Zheng L, Sugiyama H. Highly emissive deoxyguanosine analogue
814 capable of direct visualization of B-Z transition. *Chem Commun.* 2014;50(13):1573-1575.
815 doi:10.1039/c3cc48297a
816 66. Kilin V, Gavvala K, Barthes NPF, et al. Dynamics of Methylated Cytosine Flipping by
817 UHRF1. *J Am Chem Soc.* 2017;139(6):2520-2528. doi:10.1021/jacs.7b00154
818 67. Ciaco S, Gavvala K, Greiner V, et al. Thienoguanosine brightness in DNA duplexes is
819 governed by the localization of its $\pi\pi^*$ excitation in the lowest energy absorption band. *Methods*
820 *Appl Fluoresc.* 2022;10(3). doi:10.1088/2050-6120/ac6ab6
821 68. Lagoa R, Marques-da-Silva D, Diniz M, Daglia M, Bishayee A. Molecular mechanisms
822 linking environmental toxicants to cancer development: Significance for protective interventions
823 with polyphenols. *Semin Cancer Biol.* 2022;80:118-144. doi:10.1016/j.semcancer.2020.02.002
824 69. Hantho JD, Strayer TA, Nielsen AE, Mancini RJ. An Enzyme-Directed Imidazoquinoline
825 for Cancer Immunotherapy. *ChemMedChem.* 2016;11(22):2496-2500.
826 doi:10.1002/cmdc.201600443
827 70. Kauffman EC, Liu H, Schwartz MJ, Scherr DS. Toll-Like Receptor 7 Agonist Therapy with
828 Imidazoquinoline Enhances Cancer Cell Death and Increases Lymphocytic Infiltration and
829 Proinflammatory Cytokine Production in Established Tumors of a Renal Cell Carcinoma Mouse
830 Model. *J Oncol.* 2012;2012:103298. doi:10.1155/2012/103298
831 71. Li H, Van Herck S, Liu Y, et al. Imidazoquinoline-Conjugated Degradable Coacervate
832 Conjugate for Local Cancer Immunotherapy. *ACS Biomater Sci Eng.* 2020;6(9):4993-5000.
833 doi:10.1021/acsbmaterials.0c00485
834 72. Avendaño C, Menéndez JC. Chapter 12 - Biological Therapy of Cancer. In: Avendaño C,
835 Menéndez JC, eds. *Medicinal Chemistry of Anticancer Drugs (Second Edition)*. Elsevier; 2015:561-
836 593. doi:10.1016/B978-0-444-62649-3.00012-0
837 73. Rottach A, Frauer C, Pichler G, Bonapace IM, Spada F, Leonhardt H. The multi-domain
838 protein Np95 connects DNA methylation and histone modification. *Nucleic Acids Res.*
839 2010;38(6):1796-1804. doi:10.1093/nar/gkp1152
840 74. Zhang J, Gao Q, Li P, et al. S phase-dependent interaction with DNMT1 dictates the role of
841 UHRF1 but not UHRF2 in DNA methylation maintenance. *Cell Res.* 2011;21(12):1723-1739.
842 doi:10.1038/cr.2011.176
843 75. Mancini M, Magnani E, Macchi F, Bonapace IM. The multi-functionality of UHRF1:
844 epigenome maintenance and preservation of genome integrity. *Nucleic Acids Research.*
845 2021;49(11):6053-6068. doi:10.1093/nar/gkab293
846 76. Bronner C, Fuhrmann G, Chédin FL, Macaluso M, Dhe-Paganon S. UHRF1 Links the
847 Histone code and DNA Methylation to ensure Faithful Epigenetic Memory Inheritance. *Genet*
848 *Epigenet.* 2010;2009(2):29-36.
849 77. Patnaik D, Estève PO, Pradhan S. Targeting the SET and RING-associated (SRA) domain of
850 ubiquitin-like, PHD and ring finger-containing 1 (UHRF1) for anti-cancer drug development.
851 *Oncotarget.* 2018;9(40):26243-26258. doi:10.18632/oncotarget.25425
852 78. Ferguson LR, Denny WA. Genotoxicity of non-covalent interactions: DNA intercalators.
853 *Mutat Res.* 2007;623(1-2):14-23. doi:10.1016/j.mrfmmm.2007.03.014
854 79. Houliston RS, Lemak A, Iqbal A, et al. Conformational dynamics of the TTD-PHD histone
855 reader module of the UHRF1 epigenetic regulator reveals multiple histone-binding states, allosteric
856 regulation, and druggability. *J Biol Chem.* 2017;292(51):20947-20959.
857 doi:10.1074/jbc.M117.799700
858 80. Qin W, Wolf P, Liu N, et al. DNA methylation requires a DNMT1 ubiquitin interacting
859 motif (UIM) and histone ubiquitination. *Cell Res.* 2015;25(8):911-929. doi:10.1038/cr.2015.72

- 860 81. Tauber M, Fischle W. Conserved linker regions and their regulation determine multiple
861 chromatin-binding modes of UHRF1. *Nucleus*. 2015;6(2):123-132.
862 doi:10.1080/19491034.2015.1026022
- 863 82. Egger G, Liang G, Aparicio A, Jones PA. Epigenetics in human disease and prospects for
864 epigenetic therapy. *Nature*. 2004;429(6990):457-463. doi:10.1038/nature02625
- 865 83. Ghoshal K, Datta J, Majumder S, et al. 5-Aza-deoxycytidine induces selective degradation
866 of DNA methyltransferase 1 by a proteasomal pathway that requires the KEN box, bromo-adjacent
867 homology domain, and nuclear localization signal. *Mol Cell Biol*. 2005;25(11):4727-4741.
868 doi:10.1128/MCB.25.11.4727-4741.2005
- 869 84. Krifa M, Leloup L, Ghedira K, Mousli M, Chekir-Ghedira L. Luteolin induces apoptosis in
870 BE colorectal cancer cells by downregulating calpain, UHRF1, and DNMT1 expressions. *Nutr*
871 *Cancer*. 2014;66(7):1220-1227. doi:10.1080/01635581.2014.951729
- 872 85. Delagoutte B, Lallous N, Birck C, Oudet P, Samama JP. Expression, purification,
873 crystallization and preliminary crystallographic study of the SRA domain of the human UHRF1
874 protein. *Acta Crystallogr Sect F Struct Biol Cryst Commun*. 2008;64(Pt 10):922-925.
875 doi:10.1107/S1744309108027462
- 876 86. Hawkins PCD, Nicholls A. Conformer generation with OMEGA: learning from the data set
877 and the analysis of failures. *J Chem Inf Model*. 2012;52(11):2919-2936. doi:10.1021/ci300314k
- 878 87. Motulsky H, Christopoulos A. Fitting Models to Biological Data Using Linear and
879 Nonlinear Regression: A Practical Guide to Curve Fitting. *undefined*. Published online 2004.
880 Accessed May 7, 2022. <https://www.semanticscholar.org/paper/Fitting-Models-to-Biological-Data-Using-Linear-and-Motulsky-Christopoulos/a95cfd8b4b3838f5535dfa77f627a50a974315d4>
- 881 88. Rizk A, Paul G, Incardona P, et al. Segmentation and quantification of subcellular structures
882 in fluorescence microscopy images using Squash. *Nat Protoc*. 2014;9(3):586-596.
883 doi:10.1038/nprot.2014.037
- 884 89. Stresemann C, Lyko F. Modes of action of the DNA methyltransferase inhibitors
885 azacytidine and decitabine. *Int J Cancer*. 2008;123(1):8-13. doi:10.1002/ijc.23607
886
887